Eur. Phys. J. B **37**, 339–344 (2004)
DOI: 10.1140/epjb/e2004-00064-6

THE EUROPEAN PHYSICAL JOURNAL B

Study of infrared phonons in the $La_{0.7}Sr_{0.3}MnO_3$ manganite by means of reflectance measurements on epitaxial films

P. Dore[1,a], A. Funaro[1], A. Sacchetti[1], M. Angeloni[2], and G. Balestrino[2]

[1] COHERENTIA-INFM and Dipartimento di Fisica, Universitá di Roma "La Sapienza", P.le A. Moro 5, 00185 Roma, Italy
[2] COHERENTIA-INFM and Dipartimento di Ingegneria Meccanica, Università di Roma Tor Vergata, Via del Politecnico 1, 00133 Roma, Italy

Received 10 October 2003 / Received in final form 7 January 2004
Published online 2 April 2004 – © EDP Sciences, Società Italiana di Fisica, Springer-Verlag 2004

Abstract. The optical phonon spectrum of the $La_{0.7}Sr_{0.3}MnO_3$ pseudocubic manganite has been investigated by means of far infrared reflectance measurements on high-quality films of different thickness grown by Pulsed Laser Deposition on $LaAlO_3$ and $SrTiO_3$ substrates. The manganite phonon spectrum, as obtained by properly modelling the measured reflectances, does not strongly depend on substrate and film thickness d. Measurements on thick-films ($100 < d < 200$ nm) on $SrTiO_3$ allow to precisely determine line profile and peak-frequency of bending ($\nu_B = 336 \pm 3$ cm^{-1}) and stretching ($\nu_S = 588 \pm 3$ cm^{-1}) phonons of the bulk manganite. The bending phonon is broadened by an extra component around 365 cm^{-1}, which strongly decreases in intensity on decreasing d below 100 nm. Although this finding is not yet fully understood, the unambiguous conclusion is that thick-films on $SrTiO_3$ are ideal samples to get detailed information on the phonon spectrum of a bulk manganite.

PACS. 63.20.-e Phonons in crystal lattice – 78.20.-e Optical properties of bulk materials and thin films – 78.30.-j Infrared and Raman spectra

1 Introduction

The intriguing physical properties of the pseudocubic $A_{1-x}A'_xMnO_3$ manganites (A is a trivalent rare-earth and A' is a divalent alkali-earth metal), where in the MnO_6 octahedra of the perovskite structure the Mn ions assume a Mn^{+3}/Mn^{+4} mixed-valence, have attracted much attention [1,2], also owing to their potential technological applications such as magnetic switches and memories [3]. Indeed, colossal magnetoresistance (CMR) occurs in many of these systems for $0.2 < x < 0.5$ around the insulator (I) to metal (M) transition at the temperature T_P, nearly coinciding with the Curie temperature T_C where the system undergoes a paramagnetic to ferromagnetic (FM) transition. A detailed understanding of these phenomena has not yet been achieved, but a key role of the double-exchange interaction, the basic mechanism responsible for electrical transport below T_C, and of the crystal lattice, through the electron-phonon coupling (EPC) triggered by Jahn-Teller distortions of the $[MnO_6]^{+3}$ octahedra, has been proposed [4]. In this scenario, correlated information on lattice dynamics, as that provided by infrared (IR) phonon studies, and on transport properties can be essential for a detailed understanding of the role of lattice distortions.

[a] e-mail: Paolo.Dore@roma1.infn.it

Three triply degenerated IR-active modes are expected in the cubic ABO_3 perovskite structure, namely, the "external" mode (ν_E) which represents a vibrating motion of the A ion against the BO_6 octahedra, and two "internal" modes, which reflect internal motions of B and O ions in the octahedron (bending mode ν_B, stretching mode ν_S). Whereas a three-component IR phonon spectrum characterises a cubic perovskite structure, a larger number of IR-active modes are expected as the crystal symmetry is reduced. Nevertheless, in the case of pseudocubic $A_{1-x}A'_xMnO_3$ manganites with $0 < x < 0.5$, the measured phonon spectrum strongly differs from a three-component spectrum only for x=0. Twenty-five IR phonons were indeed observed in a high-quality crystal of the orthorhombic $LaMnO_3$ [5], according to space-group analysis [6]. At low doping ($x < 0.2$), significant deviations from the three-component spectrum of the cubic structure have been observed. In $La_{1-x}Sr_xMnO_3$ [1,7], for example, measurements on x=0.125 [8] and x=0.15 [9] single crystals have shown that the bending mode ν_B is split in two components.

For manganites in the $0.2 < x < 0.5$ doping range, where a ferromagnetic and metallic (FMM) ground state is established, small deviations from a three-component phonon spectrum have been observed. In the case of the first IR reflectance measurements on $La_{1-x}Sr_xMnO_3$

single crystals reported by Okimoto et al. [10], no detailed phonon study was performed, but published data show three main phonons peaks. Their frequencies do not appreciably change on decreasing temperature, whereas (for $x > 0.17$) the low frequency contribution associated to free charge carriers strongly increases below T_C [11,12]. For the rhombohedral [7] $La_{0.7}Sr_{0.3}MnO_3$ (T_C=370 K), in particular, $\nu_E \cong 160$, $\nu_B \cong 335$, and $\nu_S \cong 590$ cm^{-1} (see Fig. 9 in Ref. [10]). Three phonon peaks were also observed in the detailed phonon study of Kim et al. [13] on polycrystalline $La_{0.7}Ca_{0.3}MnO_3$. On decreasing temperature below T_C, both ν_B and ν_S significantly increase in frequency, while ν_E does not appreciably change. This effect was not confirmed by measurements on a $La_{0.67}Ca_{0.33}MnO_3$ single crystal [14], showing that only a redistribution of oscillator-strength between nearly degenerate components takes place on lowering temperature. The results of Kim et al. [13] have also been questioned on the basis of measurements on polycrystalline $La_{1-x}Ca_xMnO_3$ samples with x=0.35 [15] and x=0.3 [16]. In summary, definitive results on the phonon spectrum of manganites with FMM ground state are still not available, owing also to the lack of optimal samples. In measurements on polycrystalline samples the phonon peaks can indeed be broadened by inhomogeneities and disorder, and can slightly depend on sample preparation [17]. In the case of single crystals, when available, the major problems arise from the small sample surface, which must be properly polished or cleaved in order to avoid spurious results in infrared measurements [12].

Since definitive results on the phonon temperature dependence can have a key role in determining the role of EPC in the IM transition [13], the first aim of the present paper is to verify if reflectance measurements on films can provide an accurate determination of the manganite phonon spectrum. Epitaxial films with a large and high-quality surface allow indeed high-accuracy reflectance measurements, although the measured spectrum can be strongly affected by the substrate when the radiation penetration depth is larger than the film thickness.

In the present paper we report far-infrared (FIR) reflectance measurements on $La_{0.7}Sr_{0.3}MnO_3$ films grown on $LaAlO_3$ and $SrTiO_3$ substrates. It is worth to notice that, at least to our knowledge, a phonon study in manganite films has been only performed on $La_{0.7}Ca_{0.3}MnO_3$ films grown on different perovskite substrates [18]. A splitting of the bending mode, attributed to the manganite orthorhombic distortion, and a strong dependence of ν_B and ν_S on the employed substrate were observed.

Recently, manganite films, which are essential in technological applications, have been the object of an intense research since the magnetotransport properties of thin films can strongly differ from those of the bulk material. For details, we refer to a comprehensive review recently published [3]. Here we just notice that T_P significantly decreases on decreasing the film thickness d below a critical thickness d_c, but a large variety of d_c values have been reported even for the same film/substrate system [3]. The substrate-induced lattice strain in thin films has been first proposed to explain thickness effects [19]. However, according to different authors, strain effects cannot explain the thickness dependence of the film properties (see for instance Ref. [20]). Moreover, the importance of a thin "dead layer" at the film/substrate interface, whose nature is still controversial, has been pointed out (see for instance Ref. [21]). In this scenario, a further aim of the present paper is to verify, through measurements on films of different thickness, if the IR phonon spectrum can probe any substrate-induced change in the film lattice structure.

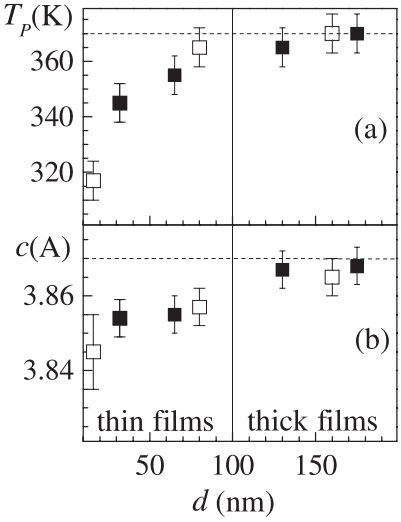

Fig. 1. T_P (panel a) and c lattice-parameter (panel b) as a function of thickness d for $La_{0.7}Sr_{0.3}MnO_3$ films grown on STO(001) substrates. Open symbols refer to samples studied in reference [22], full symbols refer to the samples investigated in the present paper. The horizontal dashed lines represent the T_P (panel a) and c (panel b) bulk values. The vertical full line divides fully relaxed films (thick-films) from strained films (thin-films).

2 Experimental results

$La_{0.7}Sr_{0.3}MnO_3$ (LSMO) films of different thickness d were grown by Pulsed Laser Deposition on $SrTiO_3$(001) (STO) and on $LaAlO_3$(001) (LAO) substrates. For each film, the c-lattice parameter was measured by standard θ-2θ X-ray diffraction. In all film/substrate samples, the resistance measured by standard four-probe technique increases on increasing temperature and then remains nearly constant above T_P, thus providing the T_P value. Details on sample preparation and characterisation are reported in reference [22]. In the present paper, it is convenient to divide the film/substrate samples in different categories. In thick-film samples ($100 < d < 200$ nm), the c-lattice parameter and the T_P value are close to the LSMO bulk values (c = 3.870 Å, T_P = 370 K) indicating that d_c is of the order of 100 nm, i.e. that the film is completely relaxed when $d > 100$ nm. In thin-film samples ($d < d_c$), thickness effects become important: c varies and T_P decrease on decreasing d. Figure 1 shows the d dependence of c and T_P in the 10–200 nm range for the LSMO/STO

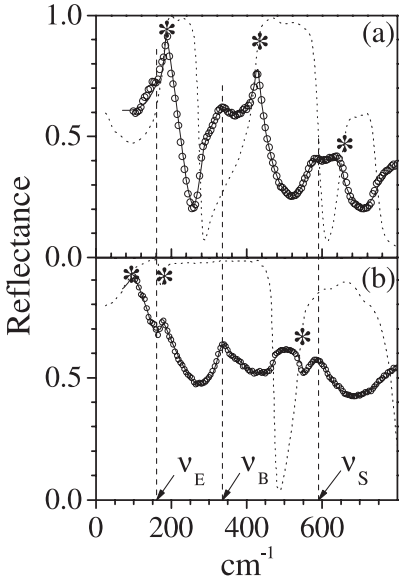

Fig. 2. (a) $R(\nu)$ of sample 450L (open symbols), best-fit curve (full line), $R(\nu)$ of LAO (dashed line). (b) $R(\nu)$ of sample 680S (open symbols), best-fit curve (full line), and $R(\nu)$ of STO (dashed line). Stars indicate the peak frequencies of the main IR-active phonons of LAO (a) and STO (b). Vertical dashed lines indicate the peak frequencies of the ν_E, ν_B, and ν_S LSMO phonons observed in bulk material (see text).

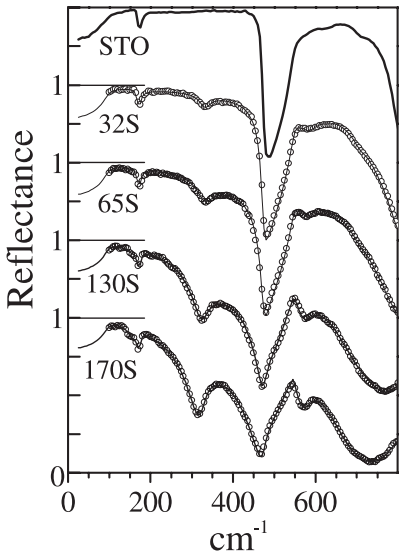

Fig. 3. $R(\nu)$ of LSMO/STO samples with $d < 200$ nm (open symbols) and best-fit curves (full lines). The $R(\nu)$ of STO is reported for easy comparison.

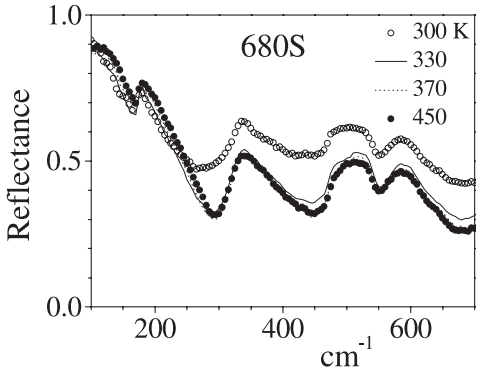

Fig. 4. $R(\nu)$ of the thick-film sample 680S at selected temperatures in the 300–450 K range.

samples studied in reference [22] and for the thin-film and thick-film samples investigated in the present paper. Hereafter, each sample will be identified by d value (in nm) and substrate (S for STO, L for LAO). Ultra-thin-film samples ($d < 10$ nm), where the "dead-layer" effect is observed [22], are not considered here since FIR reflectance measurements at near-normal incidence are not sensitive to such thin layers. On the contrary, ultra-thick-film samples ($d > 400$ nm) were prepared and studied through IR measurements, although the film crystalline quality is slightly worse than in the thick-film case.

Far-infrared reflectance measurements at near-normal incidence were performed at room temperature in the 100–800 cm^{-1} frequency range by using two interferometers equipped with different beam-splitters and detectors [23]. In the vacuum chamber of the interferometer, the sample holder can be rotated in order to measure alternatively the radiation intensity reflected at near-normal incidence by a gold surface ($I_0(\nu)$) or by the film surface ($I(\nu)$). Typically, the diameter of the light spot employed to obtain high-accuracy $R(\nu) = I(\nu)/I_0(\nu)$ reflectance spectra is of the order of 3 mm.

The $R(\nu)$ spectra of the two ultra-thick-film samples 450L (450 nm film on LAO) and 680S (680 nm film on STO), where both c and T_P are close to the bulk values, are reported in Figures 2a and 2b, respectively. The $R(\nu)$ of sample 450L is compared with that of bare LAO [24], the $R(\nu)$ of sample 680S with that of bare STO [25]. The peak frequency of the main IR-active phonons of LAO [24] and STO [25] indicated in Figure 2 show that even in ultra-thick-film samples the reflection at the film-substrate interface is not avoided. It is thus necessary to model the reflectance spectrum of the film+substrate system in order to determine the LSMO phonon spectrum (see next section). Figure 2 also shows that the ν_B and ν_S phonons observed in bulk LSMO [10] are peaked at frequencies where the substrate reflectance is nearly constant in the case of STO, while it is steeply varying in the case of LAO. Therefore, for LSMO/LAO samples, the effect of the LSMO phonons on the measured $R(\nu)$ is hardly detectable for $d < 200$ nm, as indicated by test measurements. We thus studied in detail LSMO/STO samples, in particular the thick-film (175S and 130S) and thin-film (65S and 32S) samples accurately characterised (see Fig. 1). The resulting $R(\nu)$ spectra reported in Figure 3 show that the effect of the ν_B and ν_S phonons is evident on decreasing d down to about 30 nm.

Measurements were finally performed on LSMO/STO samples at high temperatures (up to 450 K) by mounting an heater block on the sample holder. A decrease of $R(\nu)$ on increasing temperature, hardly detectable when $d <$ 200 nm, is evident for ultra-thick film samples, as shown in Figure 4 in the case of sample 680S.

3 Data analysis

In order to analyse the measured spectra, we employed a procedure which models the optical system vacuum-film-substrate-vacuum and provides exact expressions for transmittance and near-normal-near incidence reflectance of a film of thickness d on a substrate of thickness D [26]. The procedure requires a detailed knowledge of the substrate dielectric function, i.e. of its refractive indices $n_s(\nu)$ and $k_s(\nu)$. By using $n_s(\nu)$ and $k_s(\nu)$ data available for both LAO [24] and STO [25], the model $R(\nu)$ only depends on d, D, and on the refractive indices of the film $n_f(\nu)$ and $k_f(\nu)$. The standard Drude-Lorentz (DL) model for the film dielectric function $\tilde{\varepsilon}_f$ provides $n_f(\nu)$ and $k_f(\nu)$ $\left(\sqrt{\tilde{\varepsilon}_f} = n_f + ik_f\right)$ through [27]:

$$\tilde{\varepsilon}_f(\omega) = \varepsilon_1 + i\varepsilon_2 = \varepsilon_\infty - \frac{4\pi\Gamma\sigma_0}{\omega^2 + i\omega\Gamma} + \sum_{j=1}^{N} \frac{A_j^2\omega_j^2}{\omega_j^2 - \omega^2 - i\gamma_j\omega} \quad (1)$$

where $\omega = 2\pi c\nu$. We recall that the absorption spectrum is usually expressed in terms of the optical conductivity $\sigma(\omega) = \omega\varepsilon_2(\omega)/4\pi$. The DL parameters in equation (1) are high-frequency dielectric constant ε_∞, damping Γ and zero-frequency conductivity $\sigma_0 = \sigma(\omega = 0)$ in the Drude contribution accounting for free charge-carriers. Peak-frequency ν_j, intensity A_j, and damping γ_j describe the j-phonon in the sum of N Lorentzian oscillators. The resulting $R(\nu)$ model spectrum thus depend on d, D, and DL parameters. In the present case, D plays no role since the substrates are not transparent in the FIR region (only LAO becomes transmitting below 100 cm^{-1}) and thus a simplified optical system (vacuum-film-semiinfinite substrate) could be considered. We verified that the results of the procedure we utilised [26] are equivalent to those provided by a different procedure valid for the simplified optical system [28].

Good fits of all the measured $R(\nu)$ were obtained, as shown in Figures 2–3, by using $\varepsilon_\infty = 3.9$ and by considering, besides the Drude contribution and the three Lorentzian components accounting for the expected LSMO phonon lines, a fourth component around 350 cm^{-1}. A fifth component centred above 1500 cm^{-1}, accounting for mid-infrared contributions [11,12], was also introduced. For all samples, the best-fit d value is well consistent with the measured one. The LSMO optical conductivity $\sigma(\nu)$ as obtained for different samples is reported in Figure 5, showing no evident effects of the film thickness d, in particular on peak frequencies.

In the case of the thick-film sample 170S, the different components of $\sigma(\nu)$, reported in Figure 5, show that the phonon lines are superimposed to a nearly constant background described by the Drude contribution ($\sigma_0 = 220 \pm 10\ \Omega^{-1}$ cm^{-1}) and by the low-frequency tail of component 5. Owing to the limited spectral range we explored, it was not possible to obtain reliable values of the Drude damping Γ (which is higher than 1000 cm^{-1} for all samples) and of the parameters describing component 5. Figure 5 shows that the ν_E phonon is described by component 1 ($\nu_1 = 158 \pm 6$ cm^{-1}, $\gamma_1 = 33 \pm 8$ cm^{-1}, $A_1 = 4.2 \pm 0.5$), ν_S by component 3 ($\nu_3 = 588 \pm 2$ cm^{-1}, $\gamma_3 = 58 \pm 3$ cm^{-1}, $A_3 = 1.70 \pm 0.05$), while the ν_B phonon line is given by the sum of components 2 ($\nu_2 = 336 \pm 2$ cm^{-1}, $\gamma_2 = 38 \pm 2$ cm^{-1}, $A_2 = 2.52 \pm 0.05$) and 4 ($\nu_4 = 362 \pm 4$ cm^{-1}, $\gamma_4 = 80 \pm 8$ cm^{-1}, $A_4 = 2.6 \pm 0.2$). The quoted errors on the parameter values represent the range over which the parameters can be varied without changing appreciably the fit quality. It is worth to notice that components 2 and 3 are well determined, i.e. the errors on the related parameters are small since the $R(\nu)$ of the sample clearly differs from that of bare STO substrate around the peak frequencies (see Fig. 3). Component 4 is slightly more uncertain, since it is not associated to a clear feature in the measured $R(\nu)$, while large errors affect parameters describing component 1 since the low-frequency $R(\nu)$ is dominated by the reflection at the film/STO interface.

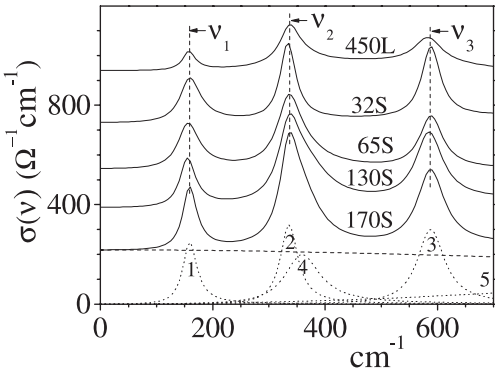

Fig. 5. Optical conductivity $\sigma(\nu)$ of LSMO (full line) as obtained for different samples. Successive curves are offset by 200 Ω^{-1} cm^{-1} for clarity. In the case of sample 170S, the $\sigma(\nu)$ components are reported (Drude component: dashed line, Lorentzian components 1–5: dotted lines). The vertical dashed lines indicate the weighted average values of ν_1, ν_2, and ν_3 (see text).

In the case of the thick-film sample 130S, parameter values (and related errors) determining the phonon spectrum do not significantly change. Peak-frequency and line-profile of the bending and stretching phonons are thus precisely determined through measurements on thick-film samples. In the case of the ultra-thick-film sample 680S, where parameter errors increase since the phonon lines are less resolved owing to lower sample quality, no significant change of phonon frequencies is observed. Also in the case of thin-film samples (65S and 32S), the peak-frequency values of the 1–3 components remain nearly constant, although the errors on the best-fit parameter values (in particular on ν_4, γ_4, and A_4) increase since the difference between the $R(\nu)$ of sample and that of bare STO reduces (see Fig. 3). We conclude that, for LSMO/STO samples, the ν_1, ν_2, and ν_3 values do not change on varying d (weighted average values are $\nu_1 = 160 \pm 10$ cm^{-1}, $\nu_2 = 336 \pm 3$ cm^{-1}, $\nu_3 = 588 \pm 3$ cm^{-1}), at least within the quoted uncertainties. In the 65S spectrum, component 4, although less determined and of reduced intensity, is essential in obtaining a good fit. On the contrary, a good

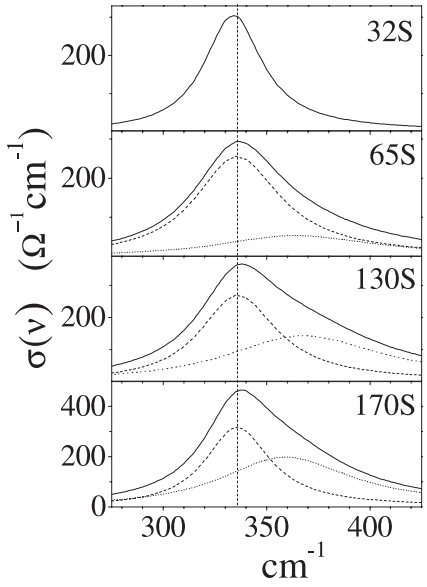

Fig. 6. Line profile (full line) of the ν_B phonon contribution. Components 2 (dashed line) and 4 (dotted line) are shown separately. Vertical dashed line indicates the peak-frequency of the ν_2 component.

fit of the 32S spectrum can be obtained with a vanishingly small A_4 value. Figure 6 shows the ν_B phonon line, given by the superposition of ν_2 and ν_4 components, for the different samples. Although the phonon line-profile is precisely determined only for thick-film samples (170S and 130S), we conclude that a clear effect of the film thickness is evident in component 4, which significantly decreases in sample 65S, and nearly vanishes in sample 32S.

The analysis of test measurements performed on LSMO/LAO samples with $d < 200$ nm shows that the phonon frequencies, although affected by large errors, are very close to those obtained for the ultra-thick-film sample 480L. Moreover, the LSMO phonon spectrum from sample 480L is very similar to those obtained from LSMO/STO samples, as shown in Figure 5. A negligible substrate dependence of the ν_2 and ν_3 best-fit values is thus observed. This finding is in disagreement with previous results obtained in the case of $La_{0.7}Ca_{0.3}MnO_3$ films on different perovskite substrates, showing a strong dependence of ν_B and ν_S on the employed substrate [18].

We finally consider the $R(\nu)$ spectra measured on the thick-film sample 680S ($T_P = 365$ K) from room temperature up to 450 K, i.e. from below to above T_P. Figure 4 shows that above 250 cm^{-1} the $R(\nu)$ intensity decreases up to a temperature of the order of 350 K and then does not appreciably change. In order to analyse high-temperature spectra, we determined $n_s(\nu)$ and $k_s(\nu)$ at each working temperature by interpolating the parameter values which determine the $\tilde{\varepsilon}(\nu)$ of STO at high temperatures [29]. The results of the fitting procedure indicate negligible changes with temperature in phonon frequencies. On increasing temperature, the change in $R(\nu)$ is mainly due to a temperature dependence of the Drude contribution, in particular to a decrease of the σ_0 value. This result is consistent with the temperature dependence of the film resistivity ρ (see Sect. 2) which significantly increases on increasing temperature up to T_P, and then remains nearly constant.

4 Discussion and conclusions

The study of FIR reflectance spectra of high-quality LSMO films shows that results obtained from LSMO/STO samples can provide detailed information on the manganite phonon spectrum. In particular, peak-frequency and line-profile of the bending and stretching phonons are precisely determined by measurements on thick-film ($100 < d < 200$ nm) samples. The peak-frequency values ($\nu_B = 336 \pm 3$ cm^{-1}, $\nu_S = 588 \pm 3$ cm^{-1}) are in good agreement with those we obtain (with lower accuracy) in the case of ultra-thick-film ($d > 400$ nm) samples, and with those observed in a LSMO single crystal ($\nu_B \cong 335$ cm^{-1}, $\nu_S \cong 590$ cm^{-1}) [10]. We conclude that FIR measurements on thick-film LSMO/STO samples allow to determine the phonon spectrum of bulk LSMO, consistently with the results of structural and resistivity measurements which indicate that thick-films are completely relaxed [22]. Our finding on the ν_B phonon line-profile, which is asymmetrized and broadened by component centred around 365 cm^{-1}, indicates that deviations from the ideal cubic structure are not negligible. This conclusion is consistent with previously reported results (see Sect. 1) for bulk $La_{1-x}Sr_xMnO_3$ and $La_{1-x}Ca_xMnO_3$ samples at different dopings, showing a splitting of the bending mode.

In the case of thin ($d < 100$ nm) LSMO/STO samples, we found that component 4, although not precisely determined, clearly decreases on decreasing d and almost vanishes when $d \cong 30$ nm. This finding, although not yet fully understood, should be related to the substrate-induced strain which determines the decrease of the c-lattice parameter observed on decreasing d below 100 nm (see Fig. 1). Since in thin epitaxial films the in-plane lattice parameters a and b match the cubic STO lattice giving rise to a square in-plane lattice [30], we guess that such strain effect might modify the lattice symmetry and, consequently, the phonon spectrum. Further studies on thin-film systems are in program in order to verify if IR measurements can accurately monitor the substrate-induced lattice changes and the possible effects of the "dead layer".

The unambiguous conclusion of the present paper is that high-quality epitaxial films (with $d > 100$ nm) on STO, which can be routinely grown with well controlled cation stoichiometry, allow to get detailed information on the IR-active bending and stretching phonons of bulk manganites. Temperature-dependent phonon studies will be of particular importance in the case of pseudocubic manganites with a FMM ground state, where results reported in the literature are contradictory (see Sect. 1). Although the present measurements collected from below to above T_P show no evident change in the phonon spectrum of the large-bandwidth [2] LSMO manganite, temperature dependent measurements should be performed on intermediate-bandwidth manganites such as

$La_{1-x}Ca_xMnO_3$ (with $0.2 < x < 0.5$). In these systems EPC has an important role [2,31], and a precise determination of the temperature dependence of the phonon spectrum could be essential for a deeper understanding of the relevance of lattice distortions on electrical transport and CMR.

References

1. *Colossal Magneto-resistance Oxides*, edited by Y. Tokura, Monographs in Condensed Matter Science (Gordon and Breach, Reading, UK, 2000), and references therein
2. E. Dagotto, T. Hotta, A. Moreo, Phys. Rep. **344**, 1 (2001), and references therein
3. A.M. Haghiri-Gosnet, J.P. Renard, J. Phys. D **36**, R127 (2003), and references therein
4. A.J. Millis, Nature **392**, 147 (1998)
5. A. Paolone, P. Roy, A. Pimenov, A. Loidl, O.K. Mel'nikov, A.Y. Shapiro, Phys. Rev. B **61**, 11255 (2000)
6. I.S. Smirnova, Physica B **262**, 247 (1999)
7. J. Hemberger, A. Krimmel, T. Kurz, H.A. Krug von Nidda, V.Y. Ivanov, A.A. Mukhin, A.M. Balbashov, A. Loidl, Phys. Rev. B **66**, 094410 (2002)
8. F. Mayr, C. Hartinger, M. Paraskevopoulos, A. Pimenov, J. Hemberger, A. Loidl, A.A. Mukhin, A.M. Balbashov, Phys. Rev. B **62**, 15673 (2000)
9. A. Paolone, P. Roy, A. Pimenov, A. Loidl, A.A. Mukhin, A.M. Balbashov, Eur. Phys. J. B **16**, 245 (2000)
10. Y. Okimoto, T. Katsufuji, T. Ishikawa, T. Arima, Y. Tokura, Phys. Rev. B **55**, 4206 (1997)
11. H.J. Lee, J.H. Jung, Y.S. Lee, J.S. Ahn, T.W. Noh, K.H. Kim, S.W. Cheong, Phys. Rev. B **60**, 5251 (1999); E. Saitoh, Y. Okimoto, Y. Tomioka, T. Katsufuji, Y. Tokura, Phys. Rev. B **60**, 10362 (1999)
12. K. Takenaka, Y. Sawaki, S. Sugai, Phys. Rev. B **60**, 13011 (1999); K. Takenaka, Y. Sawaki, R. Shiozaki, S. Sugai, Phys. Rev. B **62**, 13864 (2000)
13. K.H. Kim, J.Y. Gu, H.S. Choi, G.W. Park, T.W. Noh, Phys. Rev. Lett. **77**, 1877 (1996)
14. A.V. Boris, N.N. Kovaleva, A.V. Bazhenov, P.J.M. van Bentum, T. Rasing, S.W. Cheong, A.V. Samoilov, N.C. Yeh, Phys. Rev. B **59**, 697 (1999)
15. J.P. Franck, I. Isaac, W. Chen, J. Chrzanowski, J.C. Irwin, C.C. Homes, J. Supercond. **12**, 263 (1999)
16. R.A. Lewis, J. Supercond. **14**, 143 (2001)
17. F. Gao, R.A. Lewis, X.L. Wang, S.X. Dou, J. Alloys and Compounds **347**, 314 (2002)
18. A.V. Boris, N.N. Kovaleva, A.V. Bazhenov, A.V. Samoilov, N.C. Yeh, R.P. Vasquez, J. Appl. Phys. **81**, 5756 (1997)
19. A.J. Millis, T. Darling, A. Migliori, J. Appl. Phys. **83**, 1588 (2000)
20. M. Bibes, S. Valencia, L. Balcells, B. Martinez, J. Fontcuberta, M. Wojcik, S. Nadolski, E. Jedryka, Phys. Rev. B **66**, 134416 (2002)
21. J.Z. Sun, D.W. Abraham, R.A. Rao, C.B. Eom, Appl. Phys. Lett. **74**, 3017 (1999)
22. M. Angeloni, G. Balestrino, N. Boggio, P.G. Medaglia, P. Orgiani, A. Tebano, submitted to J. Appl. Phys.
23. S. Cunsolo, P. Dore, S. Lupi, P. Maselli, C.P. Varsamis, Infrared Phys. **33**, 539 (1992)
24. Z.M. Zhang, B.I. Choi, M.I. Flik, A.C. Anderson, J. Opt. Soc. Am. B **11**, 2252 (1994)
25. P. Dore, A.Paolone, R. Trippetti, J. Appl. Phys. **80**, 5270 (1996); P. Dore, G. De Marzi, A. Paolone, Int. J. IR and MM waves **18**, 125 (1997)
26. P. Berberich, M. Chiusuri, S. Cunsolo, P. Dore, H. Kinder, C.P. Varsamis, Infrared Phys. **34**, 269 (1993)
27. F. Wooten, *Optical Properties of Solids* (Academic Press, London, 1972)
28. L.D. Landau, E.M. Lifshitz, *Electrodynamics of Continuous Media* (Pergamon Press, New York, 1984)
29. J.L. Servoin, Y. Luspin, F. Gervais, Phys. Rev. B **22**, 5501 (1980)
30. A. de Andres, J. Rubio, G. Castro, S. Taboada, J.L. Martinez, J.M. Colino, Appl. Phys. Lett. **83**, 713 (2003)
31. P. Postorino, A. Congeduti, P. Dore, F.A. Gorelli, A. Sacchetti, L. Ulivi, A. Kumar, D.D. Sarma, Phys. Rev. Lett. **91**, 175501 (2003)